THE ASTROPHYSICAL JOURNAL, 242:359–373, 1980 November 15

RADIATION SIGNATURES FROM A LOCALLY ENERGIZED FLARING LOOP

A. GORDON EMSLIE
Harvard-Smithsonian Center for Astrophysics; and Institute for Plasma Research, Stanford University

AND

LOUKAS VLAHOS
Department of Physics and Astronomy, University of Maryland
Received 1980 February 21; accepted 1980 May 21

ABSTRACT

We calculate the radiation signatures from a locally energized solar flare loop, at a variety of wavelengths. Our calculations depend strongly on the physical properties of the energy release mechanism which we qualitatively discuss.

The model is found to be consistent with hard X-ray, microwave, and EUV observations for plausible source parameters. From the observed GHz microwave spectrum, we deduce that a suprathermal tail of high energy electrons is created by the primary energy release; by modeling the responsible acceleration mechanism as an effective large-scale electric field, we find that the number of energetic charged particles ejected into the interplanetary medium in the model is also consistent with observation.

An important prediction of the model is that the intrinsic (i.e., neglecting photospheric backscatter) polarization of the hard X-ray burst should increase significantly over the photon energy range 20 keV$\lesssim\varepsilon\lesssim$100 keV. This feature is not present in any other flare model hitherto presented, and the use of this, and other suggested observational diagnostics, to determine the various model parameters is discussed.

Subject headings: hydromagnetics — plasmas — Sun: corona — Sun: chromosphere — Sun: flares — Sun: X-rays

I. INTRODUCTION

In the theoretical modeling of solar flares, there are three fundamental topics of interest: (i) the details of the mechanism which converts magnetic energy to plasma kinetic energy and/or particle acceleration; (ii) the means by which this energy is transported from the primary energy release site to other regions of the solar atmosphere; and (iii) the resulting radiation signatures from the energized atmosphere. By its very nature, the basic physics of primary energy release occurs below the limit of current instrumental resolution; thus one of the most effective diagnostics of the properties of the mechanism of energy release is the radiation produced as a result of the transport of energy from the primary release site to other regions of the atmosphere. Over the past few years there has been a considerable effort to coordinate flare theory and observation, with a view to discriminating between various energy release and transport mechanisms (see, e.g., Švestka 1976; Sturrock 1980; Brown and Smith 1980; Emslie and Rust 1980).

Observations from *Skylab* (e.g., Widing and Cheng 1974) have conclusively demonstrated that the geometry of the energy release region is often that of a loop, with the energy release apparently occurring near the top of this structure in the majority of cases (Cheng and Widing 1975). Theoretical models both of the primary energy release and of the energy transport through the atmosphere which employ looplike geometries have been pursued by, e.g., Spicer (1976, 1977*a*) and Machado and Emslie (1979), respectively.

In this paper we therefore investigate in some detail the various radiation signatures to be expected from a flare model in which energy is released locally at the top of a coronal loop. We shall concentrate principally on signatures of the impulsive phase, since these signatures are more closely related to the fundamental energy release process. The exact mechanism of energy release is not directly relevant here; possibilities include magnetic field annihilation near singular ($\mathbf{k}\cdot\mathbf{B}=0$) points by the tearing mode instability (Furth, Killeen, and Rosenbluth 1963; Spicer 1976, 1977*a*; Van Hoven 1979). The feasibility of such an energy release model at producing hard X-ray bursts thermally has been explored by Brown, Melrose, and Spicer (1979), Smith and Lilliequist (1979), Emslie and Brown (1980), Smith and Auer (1980), Brown, Craig, and Karpen (1980), and Emslie (1981); such models are now generally accepted to seriously rival the long-accepted nonthermal interpretation of these bursts (in terms of bremsstrahlung from a beamed energetic electron flux—see Brown 1971).

The present paper is intended as a sequel to the work of Vlahos and Papadopoulos (1979; hereafter VP). These authors schematically illustrated the way in which the various flare radiation signatures associated with such a point-energy-release-at-the-top-of-a-loop model would be produced (their Fig. 5). In § II of the present paper we review the basic points of the model and parametrize its properties. By making only two strong constraints on the energy release process, we find that we can completely specify the physics of the energy transport during the impulsive phase and so construct the predicted radiation signatures at a variety of wavelengths, in terms of the physical parameters of the flaring loop. In §§ III–V we discuss the hard X-ray, microwave, and EUV signatures associated with the model and test for consistency with observational data. Section VI unifies these results and deduces observational constraints on certain model parameters, in particular on the features of the high energy electron tail which precipitates into the chromosphere (see § II). Using this information, we deduce in § VII the minimum required strength of the electric field created by the magnetic reconnection process in the energy release site and thus arrive at the number of particles which subsequently escape along open field lines into the interplanetary medium or upper corona. Finally, in § VIII, we summarize the results obtained and point to future observational data which will help better define the characteristics of this type of solar flare model.

II. THE MODEL

A schematic of the model is shown in Figure 1. This type of model has been invoked by other authors, notably in connection with hard X-ray bursts (e.g., Brown, Melrose, and Spicer 1979; Smith and Lilliequist 1979; Smith and Auer 1980; Emslie and Brown 1980). The basic model assumptions are as follows:

1. The energy is released in a volume small compared to the total volume of the loop. This can qualitatively be explained by the fact that in a bipolar loop the magnetic field is most unstable around the portion of the loop which has the weakest magnetic field strength (see, e.g., Appendix A of Spicer 1976).

2. The plasma electrons are heated impulsively (e.g., the rate of energy release in region I is much greater that the rate of energy loss) up to a temperature $T_e^{\rm I}$, by a mechanism that preferentially deposits its energy on electrons, so that $T_e^{\rm I} \gg T_i^{\rm I}$, where $T_i^{\rm I}$ is the ion temperature.

We also use one more simplification which is not crucial to our model, but will assist in our calculations: we assume that the energy is released at the top of the loop. This assumption is in accordance with the observations of Cheng and Widing (1975).

The exact electron velocity distribution in region I depends on the details of the energy release mechanism which we do not address in this study. In the present paper we therefore make use of two convenient parametric representations which represent two different ways of transferring magnetic energy to plasma kinetic energy.

a) The magnetic energy primarily heats the plasma (i.e., $\sim$100% of magnetic energy goes toward increasing the random motion of the plasma particles). The electron velocity distribution in this case will thus be represented by a Maxwellian with temperature $T_e^{\rm I}(r)$, where r measures the distance along the loop from the point of energy release. In practice, the requirements of the model (in particular, the condition that the unstable conduction fronts [Fig. 1; see below] be at marginal stability; see, e.g., Brown, Melrose, and Spicer 1979) make the scale length r_0 associated

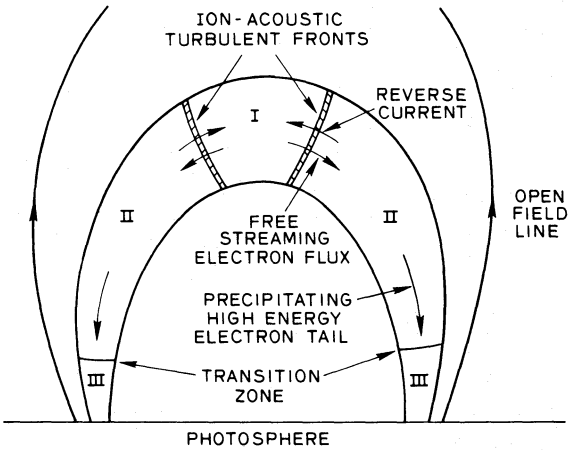

FIG. 1.—Schematic of the flare model (cf. Vlahos and Papadopoulos 1979). In region I the energy release occurs by magnetic reconnection, causing hot electrons to stream into region II. The associated reverse current builds up turbulent plasma fronts as shown; this restricts the free streaming of the hot electrons and sets up a marginally stable state, with very energetic electrons ($v > v_u$) precipitating out of region I to partially balance the reverse current. Region III represents the dense (chromospheric) region of the loop.

with the temperature variation very large (Emslie and Brown 1980); thus $T_e^{\rm I}$ will be considered constant, except where this is clearly no longer sufficient for our purposes (e.g., in the discussion of hard X-ray polarization—Emslie and Brown 1980; § III). The velocity distribution in this case (assumed to be strictly one-dimensional along the axis of the loop) is thus given by

$$f_1(v)=\left(\frac{2}{\pi}\right)^{\frac{1}{2}} n \frac{\exp\left[-v^2/2(v_e^{\rm I})^2\right]}{v_e^I} \text{ cm}^{-3}(\text{cm s}^{-1})^{-1}, \tag{1}$$

where n is the local number density [which we assume to be constant along the loop—note the small [$\sim$5%] variation in $n(r)$ obtained by Smith and Lilliequist 1979 and the approximate pressure equilibrium found by Smith and Auer 1980 in their hydrodynamical treatments of the energy release region], and $v_e^{\rm I}$ is the mean electron thermal velocity in region I.

b) The magnetic energy primarily goes into heating, with the exception of a small percentage which increases the energy of the electrons at the high energy tail of Maxwellian distribution. We parametrize the above physical picture by a Maxwellian up to an upper velocity limit $v_u=\beta v_e^{\rm I}$, with a power-law tail (*energy flux* spectral index δ) for $v>v_u$, where v_u is the velocity above which electrons are not confined in region I by the ion-acoustic turbulent fronts (Fig. 1; see below) and thus escape into the other parts of the atmosphere (regions II and III in Fig. 1; cf. VP). For this distribution, therefore,

$$f_2(v)=\left(\frac{2}{\pi}\right)^{\frac{1}{2}} n \frac{\exp\left[-v^2/2(v_e^{\rm I})^2\right]}{v_e^{\rm I}}, \quad v \le \beta v_e^{\rm I}$$

$$=\left(\frac{2}{\pi}\right)^{\frac{1}{2}} n \frac{\exp(-\beta^2/2)}{v_e^{\rm I}}\left(\frac{\beta v_e^{\rm I}}{v}\right)^{2\delta}, \quad v>\beta v_e^{\rm I}. \tag{2}$$

A few comments concerning the form of the distribution (2) are in order. First we note that $f_2(v)$ is not strictly normalized [$\int f(v)dv>n$ in general, the strength of the inequality depending on β and δ]; however, for plausible values of β (see Brown, Melrose, and Spicer 1979; VP) this discrepancy is readily shown to be negligible. Second, the high energy electrons will lose energy in overcoming the turbulent thermoelectric field (Smith and Brown 1980). Thus the form of the distribution for $v>\beta v_e^I$, which for the present paper is relevant only to regions II and III, is the result of a significantly different distribution in the acceleration region itself. The details of this region I distribution are beyond the scope of the present paper; but throughout what follows, it must be remembered that equation (2) is merely a convenient parametrical representation of the electron velocity distribution, chosen to give a harder spectrum in region II than the extended Maxwellian (eq. [1]) (which in itself is somewhat artificial in the light of these remarks). Finally, we note that hard X-ray spectra are well determined by direct observation only up to $\varepsilon\approx$100 keV (e.g., Hoyng, Brown, and van Beek 1976); since the energy corresponding to $v=v_u$ is significantly larger than this for plausible β and $T_e^{\rm I}$ (see Brown, Melrose, and Spicer 1979; VP), we see that δ in fact can be taken as a free parameter in our analysis. We note in passing that some evidence for spectral hardening above $\varepsilon\approx$150 keV has been deduced by Langer, Petrosian, and Frost (1980), using measurements of hard X-rays backscattered from the Earth's atmosphere; this lends some observational support for the distribution (2).

As has been extensively discussed by other authors (e.g. Brown, Melrose, and Spicer 1979; Smith and Lilliequist 1979; VP), high energy electrons will stream freely out of region I into region II (Fig. 1) at the local electron thermal velocity $v_e^{\rm I}$, due to the large collisional mean free path associated with the high ($\sim 10^8$ K) value of $T_e^{\rm I}$ (Spitzer 1962; Kahler 1971*a*, *b*, 1975). The resulting reverse current becomes unstable to plasma wave turbulence when its velocity reaches the threshold velocity for the relevant (ion-acoustic) instability, the ion sound speed $c_s\approx v_e^{\rm I}/43$. (Since $T_e^{\rm I}\gg T_i^{\rm I}$, it is the ion-acoustic, and not ion-cyclotron, instability which is relevant to this situation; see Krall and Trivelpiece 1973, and remarks at the end of this section.) The resulting plasma turbulent layer will give rise to an enhanced collision frequency, so that in fact all but the most energetic electrons ($v>v_u$) are confined to region I. In order to maintain a steady-state situation (appropriate, for example, around the peak of the impulsive phase), n_b, the number of energetic electrons which escape through the turbulent layer into region II and drive the return current, must be such that

$$n_b \lesssim n\frac{c_s}{\beta v_e^{\rm I}} \approx \frac{n}{43\beta}. \tag{3}$$

One can in fact solve for β in terms of the other source parameters using the fact that the diffusion length for electrons with velocity $v \approx v_u$ must be of order L^{I} (the length of region I); it is found (see VP) that

$$\beta = \beta_0 (L^{\mathrm{I}})^{2/5} n^{1/10} (T_e^{\mathrm{I}})^{-1/5} \tau_R^{-1/5}, \tag{4}$$

the constant β_0 being such that the (slowly varying) quantity $\beta \approx 3$. (In eq. [4], τ_R is a characteristic time associated with the energy release.)

The question of the two-stream stability of the precipitated beam ($v > v_u$) and the order-of-magnitude energetics of the model have already been dealt with by VP. It is found that for the precipitated beam to be stable against growth of the two-stream instability, we must have

$$n_b/n \lesssim 10^{-4} \left[T_e^{\mathrm{I}} / T_e^{\mathrm{II}} \right]^2, \tag{5}$$

where T_e^{II} is the electron temperature in region II. This is satisfied for both distributions (1) and (2); thus the electron beam can reach the chromosphere (region III in Fig. 1).

From the above scenario the following qualitative aspects of the radiation signatures to be expected from the model around the (steady-state situation) peak of the impulsive phase are evident (see VP):

i) Hard X-ray bursts with photon energy $\varepsilon \leq E_{\min}$ ($= 1/2 m_e v_u^2$) are thermally produced within region I, while hard X-rays of all energies are emitted by thick-target bremsstrahlung of the escaping high energy tail upon interaction with the dense chromospheric layers (region III in Fig. 1); see Emslie and Brown (1980); Brown, Craig, and Karpen (1980).

ii) Microwave bursts are produced primarily by gyrosynchrotron emission of the trapped electrons in region II of the loop. The emission will be predominantly from the footpoints of this region due to the enhanced magnetic field strength there.

iii) EUV and optical radiation will be produced when the precipitating escaping high energy tail thermalizes in the chromosphere (region III).

iv) Energetic particles will be ejected into interplanetary space upon cross-field drift and subsequent reflection back along open field lines.

The model presented above is based on the assumptions (1) and (2) outlined in the beginning of this section. These assumptions are necessary and sufficient for its validity. It differs from the thick-target model (Brown 1971) only in the presence of an unstable return current *in the vicinity of region I*. The current-driven low-frequency fluctuations reduce the heat flux and the number of escaping electrons from region I considerably. But we must emphasize at this point that since the details of the energy release mechanism(s) are not known, we cannot guarantee that the assumptions (1) and (2) are always satisfied in flaring loops. For example, if $T_e^{\mathrm{I}} \approx T_i^{\mathrm{I}}$, the establishment of anomalous conduction fronts is more difficult since it requires a drift velocity for the return current $\approx 12 c_s$ (Ionson 1976). As we can see from equation (3), this may mean a significantly larger n_b/n than in the case $T_e^{\mathrm{I}} \gg T_i^{\mathrm{I}}$, which poses serious stability problems for the beam in region II (eq. [4]). On the other hand, if the energy is released simultaneously in the entire loop or gradually (e.g., rise time of a few minutes), again the above model is not valid. These variations are worth studying independently. In this paper, however, we shall henceforth focus our attention on the radiation signatures expected from the locally energized flaring loop model. In §§ III–V we shall consider signatures (i)–(iii) above, and we shall consider (iv) in § VII.

III. HARD X-RAY BREMSSTRAHLUNG

The hard X-ray bremsstrahlung yield from the type of source model considered in the present paper has been extensively dealt with by other authors (e.g., Brown, Melrose, and Spicer 1979; Smith and Lilliequist 1979; Emslie and Brown 1980; Smith and Auer 1980; Brown, Craig, and Karpen 1980). These results will here be briefly reviewed and extended to place the hard X-ray radiation signature in context with the others to be considered in subsequent sections.

The hard X-ray bremsstrahlung will be composed of two distinct parts. First there is the thermal bremsstrahlung within region I; second, the thick-target nonthermal bremsstrahlung produced by the high energy escaping tail on interaction with the dense chromospheric layers. The *spectral* characteristics of the former have been explored by Emslie and Brown (1980), Smith and Auer (1980), and Brown, Craig, and Karpen (1980). Emslie and Brown (1980) considered the instantaneous spectrum produced by the source, with no allowance for time-dependent effects, and showed that plausible X-ray spectra $I(\varepsilon)$, approximating a power-law with spectral index $\gamma \approx 3$, were obtained. Smith and Auer (1980) included a detailed hydrodynamic treatment of region I and also derived a near power-law X-ray spectrum, with $\gamma \approx 3.9$. Brown, Craig, and Karpen (1980) also allowed for the expansion of region I (at the ion sound

speed—Brown, Melrose, and Spicer 1979; Smith and Lilliequist 1979; Smith and Auer 1980), but on time scales below instrumental resolution with many such regions being produced simultaneously throughout the arch, and showed that X-ray spectra with $\gamma < 4$ could not be obtained in a purely one-dimensional model, but that by introducing more degrees of freedom (such as three-dimensional conduction from the source) the production of much harder spectra ($\gamma \approx 3$) could result, compatible with the hardest bursts ever observed (e.g., Kane 1974). The *polarization* of this thermal bremsstrahlung has been evaluated by Emslie and Brown (1980), who showed that polarizations of a few (~2–4) percent at deka-keV photon energies are produced, due to the anisotropy of the electron velocity distribution function in region I, in turn caused by the presence of a heat flux Q in this nonisothermal (see remarks in § II) region (Manheimer 1977; Spicer 1977*b*). The magnitude of this polarization was found to be relatively constant (to within a factor of 2) over the energy range 25 keV $\lesssim \varepsilon \lesssim$ 100 keV.

Spectra and polarizations for the nonthermal thick-target emission have been evaluated by a number of authors—e.g., Brown (1971, 1972, 1975), Petrosian (1973), Lin and Hudson (1976), Langer and Petrosian (1977), Bai and Ramaty (1978), Leach and Petrosian (1981). The spectrum is, of course, sensitive to the form of the electron velocity distribution in the escaping tail (i.e., for $v > v_u$), while the polarization can be quite large, up to 20% or so for the relevant energy range (for a well collimated injected beam), and again comparatively insensitive to photon energy (e.g., Brown 1972).

The composite X-ray spectral and polarization features will thus depend significantly on the ratio of thick-target to thermal bremsstrahlung at a given energy (as well as on the degree of photospheric backscatter of the radiation—Hénoux 1975; Langer and Petrosian 1977; Bai and Ramaty 1978), which in turn will depend on the model parameters introduced in § II, in particular n and $L^{\rm I}$ (see Brown, Craig, and Karpen 1980). The thermal bremsstrahlung production rate is (Culhane and Acton 1970; Somov 1975)

$$I_{\rm th}(\varepsilon) = \frac{1.63 \times 10^{-11} n^2 L^{\rm I} \exp(-\varepsilon / k_B T_e^{\rm I})}{\varepsilon (T_e^{\rm I})^{\frac{1}{2}}} \text{ photons cm}^{-2}\text{s}^{-1}\text{keV}^{-1} (\varepsilon \leq E_{\rm min}), \tag{6}$$

where $k_{\rm B}$ is Boltzmann's constant and the Gaunt factor has been approximated to unity (see Culhane and Acton 1970). The thick-target production, in the same units, is given by (Brown 1971)

$$I_{\rm tt}(\varepsilon) = \frac{2.97 \times 10^{-7}}{\varepsilon} \int_{\max(\varepsilon, E_{\rm min})}^{\infty} F(E_0)\, dE_0 \int_{\varepsilon}^{E_0} \ln \frac{1 + \sqrt{1 - \varepsilon/E}}{1 - \sqrt{1 - \varepsilon/E}}\, dE, \tag{7}$$

where the nonrelativistic Bethe-Heitler cross section (Hitler 1954) has been used, and $F(E_0)$ is the energy spectrum of the escaping tail flux ($E_0 > E_{\rm min} = \frac{1}{2} m_e v_u^2$), related to f (eqs. [1] and [2]) by

$$F(E_0) = \frac{f(v)}{m_e}\,; \quad E_0 = \tfrac{1}{2} m_e v^2, \tag{8}$$

where m_e is the electron mass. (In eqs. [6]–[8] all energies are measured in keV.)

Evaluation of (7) for the case $\varepsilon > E_{\rm min}$ is straightforward; reversing the order of double integration yields

$$I_{\rm tt}(\varepsilon)|_{\varepsilon > E_{\rm min}} = \frac{2.97 \times 10^{-7}}{\varepsilon} \int_{\varepsilon}^{\infty} \ln \frac{1 + \sqrt{1 - \varepsilon/E}}{1 - \sqrt{1 - \varepsilon/E}}\, dE \int_{E}^{\infty} F(E_0)\, dE_0. \tag{9}$$

Substituting for $F(E_0)$ in the two cases considered (see eqs. [1] and [2]), we derive, after some manipulation (cf. Brown 1971),

$$I_{\rm tt}(\varepsilon)|_{\varepsilon > E_{\rm min}} = \frac{1.08 \times 10^{6} n}{\varepsilon (T_e^I)^{\frac{1}{2}}} \times \begin{cases} (k_{\rm B} T_e^I)^2 \exp\left[\dfrac{-\varepsilon}{k_{\rm B} T_e^I}\right] K_0\left(\dfrac{\varepsilon}{k_{\rm B} T_e^I}\right), & \text{(10a)} \\ e^{-\beta^2/2} \dfrac{B(\delta - 2, \frac{1}{2})}{(\delta - 1)(\delta - 2)} E_{\rm min}^{\delta} \varepsilon^{2-\delta}, & \text{(10b)} \end{cases}$$

where the upper line refers to the distribution (1) and the lower to the distribution (2), $K_0(x)$ is the modified Bessel function of the second kind of order zero (Gradshteyn and Rhyzik 1965, formula 3.364 [3]), and B is the Beta function.

For photon energies $\varepsilon < E_{\min}$ the integration of (7) is not so straightforward; however, a useful approximation may be obtained by neglecting quantities of order $(\varepsilon/E)^2$ and higher; we obtain

$$I_{tt}(\varepsilon)|_{\varepsilon<E_{\min}} = \frac{1.08\times10^{6} n}{\varepsilon (T_e^{\rm I})^{\frac{1}{2}}} \times \begin{cases} (1+\beta^2/2) e^{-\beta^2/2} (k_{\rm B} T_e^I)^2 \ln(4E_{\min}/\varepsilon), & \text{(11a)} \\ \dfrac{e^{-\beta^2/2}}{(\delta-2)} E_{\min}{}^2 \ln\left(\dfrac{4E_{\min}}{\varepsilon}\right). & \text{(11b)} \end{cases}$$

Now considering equations (11a) and (11b) in conjunction with the thermal contribution (6), we derive the following expressions for the quantity $\eta(\varepsilon) = (I_{tt}[\varepsilon]/I_{th}[\varepsilon])|\varepsilon < E_{\min}$, which is therefore related to the relative contribution of the thick-target bremsstrahlung to the total at these energies:

$$\eta(\varepsilon) = \frac{6.63\times10^{16}}{nL^{\rm I}} \exp\left[\frac{(\varepsilon - E_{\min})}{k_{\rm B} T_e^{\rm I}}\right] \ln\left(\frac{4E_{\min}}{\varepsilon}\right) (k_{\rm B} T_e^I)^2 \times \begin{cases} (1+\beta^2/2), & \text{(12a)} \\ \dfrac{\beta^4}{4(\delta-2)}. & \text{(12b)} \end{cases}$$

Equations (10a) and (10b), and (12a) and (12b), give the total bremsstrahlung yield at energies $\varepsilon > E_{\min}$, and the fractional nonthermal contribution at energies $\varepsilon < E_{\min}$, respectively. Equation (12a) can be compared to the result derived by Brown, Craig, and Karpen (1980, their eqs. [39] and [40]); identification of their function $F(\varepsilon/k_{\rm B}T_e^{\rm I})$ with the expression

$$0.663\left(1+\frac{\beta^2}{2}\right) e^{-\beta^2/2} \ln\left(\frac{2\beta^2 k_{\rm B} T_e^I}{\varepsilon}\right) \exp\left[\frac{\varepsilon}{k_{\rm B} T_e^{\rm I}}\right] \qquad (13)$$

obtains agreement.

The significance of equations (12a) and (12b) becomes apparent when we note that η can increase, for plausible source temperatures, by an order of magnitude over the energy range 25 keV$\lesssim\varepsilon\lesssim$100 keV. Thus the polarization of the composite (thermal plus thick-target) radiation will vary from low (thermal) values at low ε to moderate (thick-target) values at high ε; this large variation (see values quoted in the introductory discussion of this section) in the polarization magnitude $|\mathbf{P}|$ is not predicted by either the purely nonthermal modeling of the authors mentioned above or the purely thermal modeling of Emslie and Brown (1980) and is therefore an important diagnostic prediction of the present model. Quantitatively, we see that

$$|\mathbf{P}|(\varepsilon) = \frac{|I_{P,\rm th}(\varepsilon) \pm I_{P,\rm tt}(\varepsilon)|}{I_{\rm th}(\varepsilon) + I_{\rm tt}(\varepsilon)}, \qquad (14)$$

where the subscript P refers to the polarized component and the $\pm$ in (14) corresponds to the planes of polarization of the thermal and thick-target radiations being parallel or perpendicular respectively [note that, of course, eq. (14) is to be interpreted as giving the upper and lower bounds to $|\mathbf{P}|(\varepsilon)$; for an arbitrary angle between the above-mentioned polarization planes $|\mathbf{P}|$ will lie between the values given by eq. (14)].

Using the definition of $\eta(\varepsilon)$, equation (14) becomes

$$|\mathbf{P}|(\varepsilon) = \frac{||\mathbf{P}|_{\rm th}(\varepsilon) \pm \eta(\varepsilon)|\mathbf{P}|_{\rm tt}(\varepsilon)|}{1+\eta(\varepsilon)}, \qquad (15)$$

where $|\mathbf{P}|_{\rm th}(\varepsilon)$ and $|\mathbf{P}|_{\rm tt}(\varepsilon)$ are the polarizations of the thermal and thick-target radiation fields, respectively. Setting

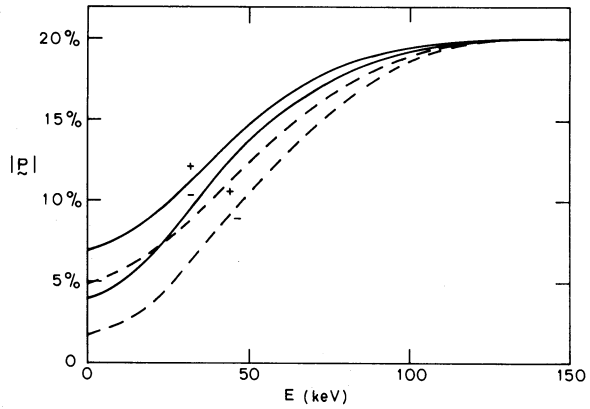

FIG. 2.—Expected variation of the intrinsic (linear) polarization of the composite (thermal plus thick-target) X-ray radiation field with photon energy ε. The solid lines correspond to the electron velocity distribution (2) (Maxwellian plus power-law tail); the dashed lines, to the distribution (1) (Maxwellian throughout). The model parameters adopted are $n=3\times10^{10}$ cm^{-3}, $L^{\rm I}=10^9$ cm, $\beta=3$ and $\delta=4$, and the intrinsic polarizations of the thermal and thick-target radiation fields are taken to be energy-independent with values 2% and 20%, respectively (see Brown 1972; Emslie and Brown 1980). The two curves in each case are upper and lower limits to $|\mathbf{P}|$ with the + and − curves corresponding to the sign in equations (14)–(16); intermediate polarizations are produced depending on the angle between the planes of polarization of the thermal and thick-target components. Note the large variation of $|\mathbf{P}|$ over a decade in photon energy: this variation is not a feature of either purely thermal (Emslie and Brown 1980) or purely non-thermal (Brown 1972) models and therefore represents an important prediction of the present model.

$|\mathbf{P}|_{\rm th}(\varepsilon)\approx2\%$ for all relevant ε (see Emslie and Brown 1980) and $|\mathbf{P}|_{\rm tt}(\varepsilon)\approx20\%$ for the same energy range (see Brown 1972), we derive

$$|\mathbf{P}|(\varepsilon)=\left|\frac{2}{1+\eta(\varepsilon)}[1\pm10\eta(\varepsilon)]\right|\text{ percent},\tag{16}$$

the behavior of which is shown in Figure 2 for the parameter set $T_e^{\rm I}=2\times10^8$ K, $n=3\times10^{10}$ cm^{-3}, $L^{\rm I}=10^9$ cm, $\beta=3$, and (where relevant) $\delta=4$ [these parameters are needed to quantify $\eta(\varepsilon)$—see eqs. (12a) and (12b)], and for both distributions (1) and (2). Note that, above $\varepsilon=E_{\rm min}\approx155$ keV, η becomes infinite and so $|\mathbf{P}|$ reduces to its thick-target value $|\mathbf{P}|_{\rm tt}$.

Observations of $|\mathbf{P}|(\varepsilon)$ are not yet sufficiently reliable (cf. Emslie and Brown 1980 and references therein) to discriminate among the thermal, nonthermal, and present hybrid models by using this diagnostic. Better observations are encouraged, for, as Figure 2 shows, accurate determination of $|\mathbf{P}|(\varepsilon)$ should be able to define the shape of the escaping tail (to be compared with that deduced from microwave observations—§ IV) or even assess the validity of the present model (since, for example, $|\mathbf{P}|$ cannot be large for small ε in the context of the present model for any reasonable set of model parameters).

IV. MICROWAVE BURSTS

In the model considered in the present paper, microwave bursts will be produced primarily in region II (see Fig. 1), for three reasons. First, region II provides a much greater emission measure than region I; second, the gyrothermal absorption of the first harmonics, being proportional to T_e (Bekefi 1966), is much weaker in region II than in region I; and third, the mildly relativistic electrons responsible for the microwave emission are reflected from the footpoints (where the magnetic field is higher) and so do not escape into region III. Note that Mätzler (1978) and Dulk, Melrose, and White (1979) have recently suggested region I (or the equivalent) as the source of the microwave emission; however, these authors neglect the escape of energetic electrons from this region and therefore their results do not hold in the context of the present model (see § II).

The microwave power at angular frequency ω can be calculated from the equation of transfer (Bekefi 1966)

$$I_{0,e}(\omega)=\frac{j_{0,e}(\omega)}{\mu^2 a_{0,e}(\omega)}\left[1-\exp\{-a_{0,e}(\omega)L^{\rm II}\}\right],\tag{17}$$

where the subscripts zero and e refer to the ordinary and extraordinary modes, respectively; $L^{\rm II}$ is the radiation path

length in the source (region II); μ is the refractive index, given by the usual relation

$$\mu^2 = 1 - (\omega_{pe}/\omega)^2, \tag{18}$$

ω_{pe} being the electron plasma frequency; and the emission and absorption coefficients are given by

$$j_{0,e}(\omega) = \int f(\mathbf{p}) \xi_{0,e}(\omega, \mathbf{p}) d^3\mathbf{p}, \tag{19}$$

$$a_{0,e}(\omega) = \frac{-8\pi^3 c^2}{\omega^2 \mu^2} \int \frac{\partial f}{\partial E} \xi_{0,e}(\omega, \mathbf{p}) d^3\mathbf{p}. \tag{20}$$

In equations (19) and (20), $f(\mathbf{p})$ is the electron momentum distribution function, readily deduced from either (1) or (2) as appropriate, c is the velocity of light, and the emissivities $\xi_{0,e}$ are given by

$$\xi_{0,e}(\omega, \mathbf{p}) = \frac{e^2\omega^2}{2\pi c} \sum_{s=1}^{\infty} \left[\left(\frac{\cos\theta - u_{\parallel}}{\sin\theta} \right)^2 J_s^2(a) \pm u_{\perp}^2 [J_s'(a)]^2 \right] \delta(b), \tag{21}$$

where, in turn, $a = (\omega/\omega_H)(v/c)\sin\theta$, $b = s\omega_H - \omega(1 - u_{\parallel})$, $u_{\parallel} = (v/c)\cos\theta$, $u_{\perp} = (v/c)\sin\theta$ (θ being the pitch angle of the electron velocity vector to the magnetic field **B**), $\omega_H = (eB/m_e c)$ is the electron gyrofrequency, $J_s(x)$ is the Bessel function of order s, and δ is the Dirac delta-function.

We have evaluated the resulting microwave spectra $I_t(\nu) = I_0(\nu) + I_e(\nu)$ ($\nu = \omega/2\pi$) for distributions (1) and (2), assuming a region II electron temperature $T_e^{II} = 2 \times 10^6$ K, a magnetic field strength $|\mathbf{B}|$ ranging from 100 gauss at the top of region II to 500 gauss at the footpoints, $\beta = 3$, and (for the latter case) $\delta = 4$, for a variety of T_e^I values; these are shown in Figures 3*a* and 3*b*, respectively. Similar calculations have been performed previously by Ramaty (1969) and Takakura (1972). We note that the spectrum produced by the Maxwellian distribution (1) is characterized by a steep cutoff at frequencies around 7–8 GHz, a feature absent from the spectra corresponding to the distribution (2). This result is significant, because Guidice and Castelli (1973), in an analysis of a large number of bursts, found that 80–90% of observed impulsive phase spectra do not exhibit this sharp cutoff at high frequencies. Thus it appears that the escaping tail is better described by a power-law distribution (2) than an extended Maxwellian (1). We shall return to this point in §§ VI and VII.

V. EUV BURSTS AND CHROMOSPHERIC HEATING

It is well established (e.g., Kane and Donnelly 1971) that broad-band (10 Å$\lesssim\lambda\lesssim$1030 Å) EUV radiation in flares originates in relatively dense layers of the atmosphere. In the flare model considered here, this radiation will be excited by the collisional degradation of the escaping high-energy tail in region III (chromospheric densities are so

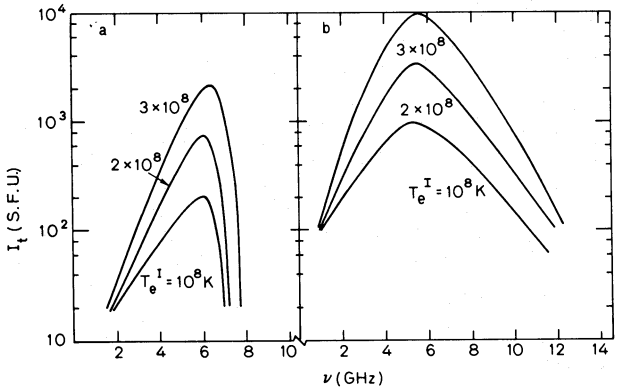

FIG. 3.—Microwave spectra for (*a*) electron velocity distribution (1), and (*b*) electron velocity distribution (2), for a source density $n = 3 \times 10^{10}$ cm^{-3} (region I) and region I electron temperatures as indicated. Note the sharp falloff in $I_t(\nu)$ at the high-frequency end of the spectrum in case (*a*); this feature is not present in case (*b*) and has important implications for the shape of the escaping high energy tail (see discussion in § IV).

high that the reverse-current ohmic losses are negligible by comparison [see Emslie 1980] and other energy sources to this region of the atmosphere are in all probability negligible, at least in the impulsive phase of the flare [cf. discussion in § VI]). In this section we therefore calculate the heating produced by the collisional interaction of the escaping tail with the chromosphere and compare it with observation.

The thick-target heating rate I_B (ergs $cm^{-3}s^{-1}$) corresponding to an arbitrary electron flux input $F(E_0)$ (particles $cm^{-2}s^{-1}$) has been given by Emslie (1978; see also Brown 1973); adopting a fully ionized target model gives

$$I_B(N) = Kn_c \int_{E^*}^{\infty} \frac{F(E_0)\,dE_0}{E_0(1-3KN/E_0^2)^{2/3}}, \tag{22}$$

where n_c (cm^{-3}) is the ambient chromospheric density, N (cm^{-2}) is the proton column density of the overlying atmosphere,

$$N = \int_z^{\infty} n_c(z)\,dz,$$

z being the height in the atmosphere, E^* is the lower cutoff in the electron energy spectrum at depth N, given by (Emslie 1978)

$$E^* = \max\left[E_{\min}, (3KN)^{\frac{1}{2}}\right], \tag{23}$$

and $K = 2\pi e^4 \ln\Lambda$, e(e.s.u.) being the electronic charge and $\ln\Lambda$ the Coulomb logarithm (see Spitzer 1962).

The total power deposited below depth N_0 is thus (see Emslie, Brown, and Donnelly 1978)

$$Q_e(N_0) = \int_{N_0}^{\infty} \frac{I_B\,dN}{n_c} = K\int_{N_0}^{\infty}\int_{E^*}^{\infty} \frac{F(E_0)\,dE_0\,dN}{E_0(1-3KN/E_0^2)^{2/3}} \text{ ergs cm}^{-2}\text{s}^{-1}. \tag{24}$$

This expression was evaluated numerically for both distributions (1) and (2). In Figure 4 we show the results for $\beta = 3$, $\delta = 4$ (where applicable), and for region I electron temperatures $T_e^I = 10^8$, 2×10^8, and 3×10^8 K.

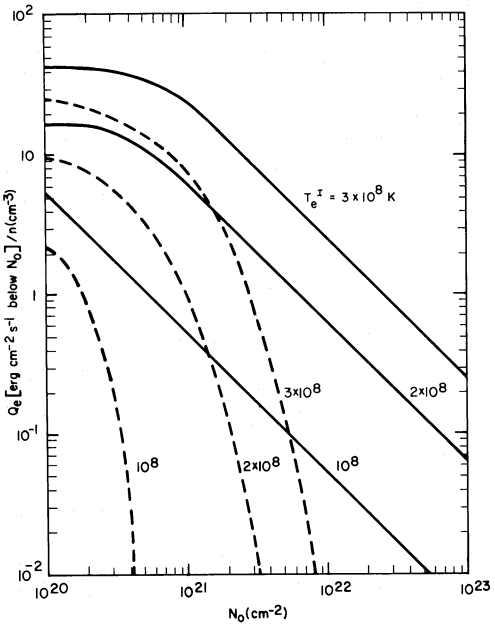

FIG. 4.—Thick-target collisional energy deposition rate Q_e (ergs $cm^{-2}s^{-1}$) below column density $N_0(cm^{-2})$, normalized to n, the electron density in region I, for various values of T_e^I. Solid lines correspond to the electron distribution (2) (Maxwellian plus power-law tail) and dashed lines to the distribution (1) (Maxwellian throughout). Note that the heating, for a given depth and source temperature, is greater when a power-law tail is present; thus the presence of this type of tail velocity distribution places a lesser demand on the primary energy release rate for compatibility of the model with EUV observations. The EUV radiation is formed in a region below $N_0 \approx 3\times10^{20}$ cm^{-2} (cf. discussion in text); thus, for reasonable source parameters, $Q_e/n \approx 10$ ergs $cm^{-2}s^{-1}$ $(cm^{-3})^{-1}$ (see [26]).

Trivially, it follows from equations (1) and (2) that $Q_e(N_0)$ scales as n. In addition, it also increases with T_e^I, as is to be expected because of the greater energy (and consequently greater heating power) of the escaping high-energy tail. For large N_0 and the distribution (2), the form of $Q_e(N_0)$ is that of a power-law with spectral index $(\delta/2-1)$; this follows because the lower limit $E^*=(3KN)^{\frac{1}{2}}$ is now appropriate (eq. [23]) and that therefore $I_B(N)\sim N^{-\delta/2}$ (Emslie 1978). For lower N_0 values, $Q_e(N_0)$ approaches a limiting value

$$Q_{\rm tot}=\int_{E_{\rm min}}^{\infty} F(E_0)v(E_0)E_0 dE_0.$$

Typical broad-band EUV fluxes in large flares are less than ~ 1 erg cm^{-2} s^{-1} at the Earth (Kane and Donnelly 1971; Emslie, Brown, and Donnelly 1978). Assuming that there are no directional effects in the EUV source (see Donnelly and Kane 1978), this corresponds to a radiated EUV power of 3×10^{27} ergs, so that in order to produce this flux from an electron injection area A, and amount of energy

$$Q_{\rm EUV}\approx \frac{3\times 10^{27}}{A} \text{ ergs cm}^{-2}\text{s}^{-1} \tag{25}$$

must be deposited per unit electron injection area. This figure is directly comparable to the results of Figure 4, due to the lack of other contributors to the radiative energy loss at the depths where the bulk of the electron power is deposited (see Emslie, Brown, and Donnelly 1978).

One of the crucial parameters in the comparison of $Q_e(N_0)$ with $Q_{\rm EUV}$ is N_c, the column density at the top of the EUV emitting layer [because of the rapid falloff of $Q_e(N_0)$ with N_0, the amount of energy passing *through* this layer is negligible by comparison]. Emslie, Brown, and Donnelly (1978) estimated N_c from purely theoretical considerations based on the radiative instability of flare plasma above temperatures $\sim 6\times 10^4$ K in Brown's (1973) analysis of electron-heated chromospheres, and derived a value of $N_c\approx 1.5\times 10^{20}$cm^{-2} (see also Brown, Canfield, and Robertson 1978). However, *empirical* flare models (e.g., Machado and Linsky 1975; Lites and Cook 1979; Machado and Emslie 1979; Machado *et al.* 1980) place this level somewhat deeper, nearer to 5×10^{20}cm^{-2} in moderately large flares; this discrepancy between theory and observation is probably due to the exclusion of terms such as Lα back-warming in the energy balance (see Machado and Emslie 1979; Machado *et al.* 1980; Emslie, Brown, and Machado 1981). Whether such extra heating terms are important in the *impulsive* phase of the flare is not entirely clear; however, it is evident from Figure 4 that, except for very low values of T_e^I, the distinction is not too important (physically this is because electrons with the minimum energy $E_{\rm min}$ of the escaping tail thermalize principally at depths $N\gtrsim 10^{21}$cm^{-2} and that therefore the heating between $N\approx 1.5\times 10^{20}$ and 5×10^{20}cm^{-2} is very small).

From Figure 4 with N_0 in the relevant range and a typical $T_e^I=2\times 10^8$ K, we see that $Q_e/n\approx 10$ ergs cm^{-2}s^{-1}(cm^{-3})$^{-1}$, almost irrespective of whether distribution (1) or distribution (2) is adopted (although we note that Q_e/n is slightly higher for the latter, which means that an escaping high energy tail with a power-law spectrum is less demanding on the primary energy release than a simple extended Maxwellian distribution). Thus, for Q_e/n to tally with $Q_{\rm EUV}$, we clearly must have

$$nA\gtrsim 3\times 10^{26}\text{cm}^{-1}. \tag{26}$$

We shall return to this result in the next section; for the present, however, we note in passing that $Q_e(N_0)$ is much more sensitive to the electron velocity distribution adopted at greater $N_0(\gtrsim 10^{21}$cm^{-2}; cf. remarks above). Thus radiation diagnostics (e.g., Hα) from this region of the flare are potentially useful in defining source parameters which are not constrained by the observed EUV emission. Treatment of this optically thick radiative transfer problem is, however, beyond the scope of the present paper.

VI. OBSERVATIONAL CONSTRAINTS ON THE SOURCE PARAMETERS

In §§ III–V we have derived the radiation signatures to be expected from the loop model of § II, and where possible their relation to existing observations. Although further observation along the lines suggested is necessary to arrive at strong diagnostic conclusions concerning this type of flare model, we can still at this stage make a few pertinent statements here.

As discussed in § III, hard X-ray polarization observations are at present much too crude to deduce the spectral form of the high energy escaping tail; however, the form of the GHz microwave spectra in Figures 3*a* and 3*b*, when compared with observation, definitely (§ IV) seem to point toward a power-law velocity distribution in the tail, and not simply an extended Maxwellian (see also Langer, Petrosian, and Frost 1980). This has important implications for the energy release mechanism in region I; in particular, an electric field must be established to accelerate the tail electrons. We shall return to this matter in § VII.

A second observational constraint is provided by the EUV observations through equation (26). The strength of this constraint is, however, limited somewhat by our knowledge of the precise form of the energy balance in the EUV emitting region. As discussed in § V, empirical modeling of flare regions strongly suggests that either thermal conduction or Lα back-warming (depending on whether the EUV emitting region comprises principally transition zone or chromospheric material respectively) will be important in this energy balance. However, empirical flare models invariably, at the present state of observational knowledge, refer to the postimpulsive phase of the flare, where the situation is much closer to a thermally relaxed situation than during the impulsive phase which is the principal consideration of the present paper. In particular, classical conductivity (Spitzer 1962) will not be relevant (although Somov 1979 has argued to the contrary, his remarks in fact apply to the post impulsive phase and so are not applicable here), thermal conduction being instead effected by the downward motion, at approximately the ion-sound speed c_s (Brown, Melrose, and Spicer 1979; Smith and Lilliequist 1979; Smith and Auer 1980), of the turbulent plasma fronts. Thus, during the times when the situation depicted in Figure 1 is relevant, thermal conduction and, as a result, Lα back-warming, will not be important contributors to the energy input to the EUV emitting region. We shall therefore interpret equation (26) as a strict constraint.

Equation (26) gives, for a density $n=3\times10^{10}$ cm^{-3} (see Brown, Melrose, and Spicer 1979) an electron injection area A of some 10^{16} cm^2, and a corresponding energy release volume $L^{\rm I}A\approx10^{24}$ cm^3 (for an energy release region 10^8 cm long), in good agreement with Spicer's (1976, 1977*a*) estimates for the volume in which magnetic reconnection takes place. Thus we see that, for reasonable source parameters, the EUV observations are consistent with this type of flare model. In addition the corresponding X-ray emission measure $n^2L^{\rm I}A$ is of order 10^{45} cm^{-3}, again in good agreement with observations (Crannell *et al.* 1978; Mätzler *et al.* 1978).

One more constraint (on the density of the loop) is provided by the following considerations. If the density is higher than 3×10^{11} cm^{-3}, the spectra of the microwave bursts is flatter at low frequencies (see Ramaty 1973). This structure in the microwave spectrum is usually not present in the *impulsive* phase (Guidice and Castelli 1973). On the other hand, n cannot be lower than 3×10^{10} cm^{-3}, since the gain in efficiency for producing hard X-rays becomes minimal (Smith and Lilliequist 1979). In our calculations both above and to follow we have taken the lower limit of this density range due to the extremely high magnetic field strength ($\sim$500 gauss) required to contain plasma with densities of order 3×10^{11} cm^{-3} and temperatures of order 2×10^8 K.

In summary, therefore, it appears that observations at hard X-ray, EUV, and microwave wavelengths are quite consistent with the model developed in § II and that an escaping high energy tail of electrons with a fairly shallow energy spectrum (such as a power law) is present. In the next section we shall discuss the mechanism responsible for the creation of this high energy tail and the implications for the number of interplanetary electrons produced by the model.

VII. PRODUCTION OF THE SUPRATHERMAL TAIL AND THE ESCAPE OF INTERPLANETARY ELECTRONS

Evidence has been adduced, on the basis of the observed microwave burst spectra (§ IV) for the presence of a suprathermal tail of high energy electrons which escape from region I, emit microwave radiation in region II, and subsequently thermalize in region III. We note that the presence of such a power law tail requires less total energy to be deposited in region I by the primary energy release mechanism (although whether candidate energy release mechanisms are effective at producing such an enhanced high energy component in the velocity distribution remains an open question at present). In addition, as we shall show below, such an electron velocity distribution results in a reasonable explanation of the good time correlation between hard X-ray bursts and type III radio bursts, in the 20% or so events where both hard X-ray and meter-wavelength radio emission occur (Kundu 1965). The acceleration process responsible for forming the high energy tail in region I is unknown, and we will therefore here represent it parametrically by a large scale DC electric field. In this section we will examine the role played by such an electric field $\mathcal{E}$ and estimate a lower limit to its strength (averaged over space and time). We shall also demonstrate that its presence results in an acceptable number of escaping interplanetary electrons.

It is well known that when an electric field $\mathcal{E}$ greater than the Dreicer field,

$$\mathcal{E}_{\rm D}=\frac{m_e\nu_0 v_e^I}{e}\approx10^{-15}(nT_e^{\rm I})^{\frac{1}{2}}\ \text{statvolt cm}^{-1}, \tag{27}$$

is applied to a plasma (in this case region I), collisional drag is no longer able to counteract the impressed electric force and the electrons with velocities $v\gtrsim v_c=(\mathcal{E}_{\rm D}/\mathcal{E})^{\frac{1}{2}}v_e^{\rm I}$ form a runaway stream. In eq. (27) $\nu_0=\omega_{pe}(\ln\Lambda/\Lambda)$ is the constant in the expression for the Coulomb collision frequency:

$$\nu(v)=\nu_0(v_e^{\rm I}/v)^3. \tag{28}$$

In the case of an ion-sound turbulent plasma, ν_0 is replaced by an effective collision frequency $\nu^* = \omega_{pe}(W_s/nk_B T_e^I)$, where W_s is the energy density of the turbulence; the velocity dependence of $\nu(v)$, however, remains the same as in equation (28) (Rudakov and Korablev 1966). Thus the anomalous Dreicer field is given by

$$\mathcal{E}_D^{an} = \frac{m_e \nu^* v_e^I}{e} \approx 3 \times 10^{-8} \left(\frac{W_s}{nk_B T_e^I} \right) (nT_e^I)^{\frac{1}{2}}. \tag{29}$$

The number of runaway electrons n_r is obtained by integrating over the Maxwellian:

$$\frac{n_r}{n} \approx \exp\left[\frac{-v_c^2}{2(v_e^I)^2} \right], \tag{30}$$

and these are accelerated to a maximum velocity

$$v_M \approx c \left\{ 1 - \left[1 + \frac{e\mathcal{E}L^I}{m_e c^2} \right]^{-2} \right\}^{\frac{1}{2}} \approx 3 \times 10^{10} \left\{ 1 - [1 + 5 \times 10^{-4} \mathcal{E} L^I]^{-2} \right\}^{\frac{1}{2}} \text{ cm s}^{-1}. \tag{31}$$

Note that if $\mathcal{E} < \mathcal{E}_D$, no significant suprathermal tail is produced. However, in a turbulent plasma, with $(W_s/nk_B T_e^I) \approx 10^{-5}$, we see from equation (29) that $\mathcal{E}_D^{an} \approx 10^{-3}$ statvolts cm^{-1}, so that, by equations (30) and (31), an $\mathcal{E}$ of only $0.1\mathcal{E}_D^{an} \approx 10^{-4}$ statvolts cm^{-1} is needed to yield $(n_r/n) \approx 10^{-2}$ and $v_M \approx 10$ cm s^{-1} (with $L^I \approx 10^8$ cm). These parameters are consistent with the observational inferences of §§ III–V, showing that in fact only a moderate electric field in region I is required to accelerate the required number of suprathermal electrons. Since the electrons in the escaping tail are primarily accelerated along the magnetic field lines, this tail has a velocity distribution with $v_\parallel \gg v_\perp$ (the components respectively parallel and perpendicular to the longitudinal axis of the loop), and therefore the anomalous Doppler resonance instability (loss-cone instability) is excited (see, e.g., Kadomtsev and Pogutse 1969; Liu and Mok 1977; Liu *et al.* 1977; Haber *et al.* 1978). We shall approximate the (three dimensional) velocity distribution in region II by (see Fig. 5 and § II)

$$\phi(\mathbf{v}) = \phi_{M,3}\left(\frac{v}{v_e^{II}} \right) + \left(\frac{n_b}{n} \right) \phi_{M,2}\left(\frac{v_\perp}{v_e^I} \right) \phi_p(v_\parallel), \tag{32}$$

where $\phi_{M,3}$ and $\phi_{M,2}$ are dimensionless three- and two-dimensional Maxwellians, respectively, and ϕ_p is a one-dimensional power-law type spectrum, normalized by the continuity of ϕ at $v = v_u$ (see § II), and with the dimensions of inverse velocity. The growth rate Γ (s^{-1}) of the electrostatic plasma waves excited by the anisotropic distribution (32) is (Krall and Trivelpiece 1973; Liu and Mok 1977)

$$\Gamma = \omega \sum_{s=-1,0,1} \frac{\pi^2 \omega_{pe}^2}{k^2 |k_\parallel|} \int dv_\perp v_\perp J_s^2\left(\frac{k_\perp v_\perp}{\omega_H} \right) \left[\frac{s\omega_H}{v_\perp} \frac{\partial \phi}{\partial v_\perp} + k_\parallel \frac{\partial \phi}{\partial v_\parallel} \right] \Bigg|_{v_\parallel = (\omega - s\omega_H)/k_\parallel}. \tag{33}$$

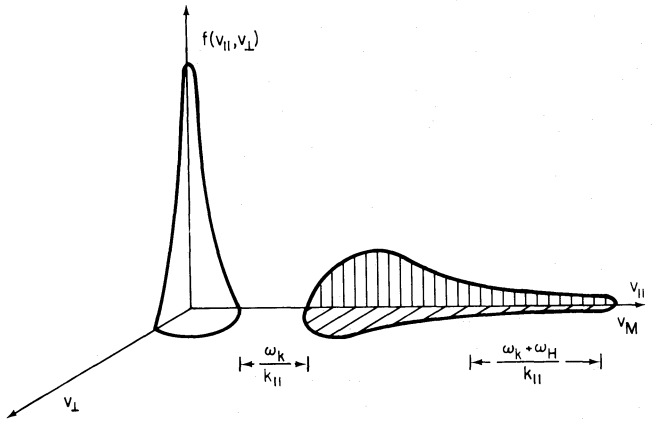

FIG. 5.—Schematic of the electron velocity distribution in region II when a strong electric field is applied in region I. Electrons in the high energy tail (*shaded*) have $v_\parallel \gg v_\perp$ and have an upper cutoff at v_M.

Since in low-lying coronal loops of the type considered in the present paper $k\rho_e \ll k\lambda_D \ll 1$ where $\rho_e = (v_e^{II}/\omega_H)$ is the electron gyroradius, we can expand the Bessel functions appearing in equation (33) in the small argument limit. Evaluating the integrals, we then obtain (Haber *et al.* 1978)

$$\frac{\Gamma}{\omega} = \frac{\pi}{4}\left(\frac{n_b}{n}\right)\left(\frac{\omega}{\omega_H}\right)\left(\frac{\omega}{k_\parallel}\right)\times\left[\left(\frac{n}{n_b}\right)\phi'_{M,3}\left(\frac{\omega}{k_\parallel v_e^{II}}\right)+\phi_p\left(\frac{\omega+\omega_H}{k_\parallel}\right)-\frac{k_\parallel (v_e^{II})^2}{2\omega_H}\phi'_p\left(\frac{\omega+\omega_H}{k_\parallel}\right)-\phi_p\left(\frac{\omega-\omega_H}{k_\parallel}\right)\right], \quad (34)$$

where a prime denotes differentiation with respect to v. The significance of the various terms in equation (34) has been given by Haber *et al.* (1978), who note that the dominant term is the second, the wave growth due to energy transfer from the $s=-1$ anomalous Doppler resonance. Thus

$$\frac{\Gamma}{\omega} \approx \frac{\pi}{4}\left(\frac{n_b}{n}\right)\left(\frac{\omega}{\omega_H}\right)\left(\frac{\omega}{k_\parallel}\right)\phi_p\left(\frac{\omega+\omega_H}{k_\parallel}\right), \quad (35)$$

provided, of course, that $[(\omega+\omega_H)/k_\parallel]$ does not exceed v_M.

Since $\omega/k_\parallel \approx 3v_e^{II}$ (see Haber *et al.* 1978), using the definition of ϕ_p (see § II), we obtain, with $\omega \approx \omega_{pe} \approx \omega_H/3$, and $\beta \approx 3$,

$$\Gamma \approx (n_b/n)(v_e^{II}/v_e^{I})\omega_{pe}. \quad (36)$$

For $(n_b/n)\approx 10^{-2}$ and $(v_e^{I}/v_e^{II})\approx 10$ (see § II), we obtain

$$\Gamma \approx 10^{-3}\omega_{pe}; \quad (37)$$

or, for a plasma density $n \approx 3\times 10^{10}$ cm^{-3},

$$\Gamma \approx 10^{7}\ \mathrm{s}^{-1}. \quad (38)$$

Thus we see that the growth time of the electron cyclotron waves is very much shorter than the loop transit time of an electron, i.e., the instability saturates well before the electron beam can reach the chromosphere.

Since the anomalous Doppler resonance instability diffuses, through pitch angle scattering, the high energy electrons in the tail from a distribution in which $v_\parallel \gg v_\perp$ to one in which $v_\parallel \approx v_\perp$, the number of trapped particles in the loop will radically increase (note, however, that $v_\parallel$ is not affected to the same degree as $v_\perp$; thus the analyses of the preceding sections are not substantially changed by the considerations of the present section). Electrons will stay out of the precipitating loss cone if

$$v_\parallel/v_\perp \lesssim (\delta B_l/B_l)^{\frac{1}{2}}, \quad (39)$$

where δB_l reflects the change in the longitudinal magnetic field B_l within L^{II}. The number of trapped particles is obtained by integrating the velocity distribution between velocities $(\omega+\omega_H)/k_\parallel$ and v_M; we find that, for plausible distributions and source parameters, approximately 10% of the beam particles are trapped, so that (see Vlahos 1979) $(n_{tr}/n)\approx 10^{-3}$, n_{tr} being the number density of trapped particles.

Once trapped, the electrons drift perpendicular to both $\boldsymbol{B}$ and $\boldsymbol{R}$ (the outward curvature radius vector) with velocity

$$v_D = \frac{\frac{1}{2}m_e c v_\perp^2}{eBR} \approx \frac{3\times 10^{12}}{BR}\ \mathrm{cm\ s^{-1}}, \quad (40)$$

and the number of particles drifting across the loop to open magnetic field lines is

$$N_{esc} = \left(\frac{n_{tr}}{n}\right) n 2\pi R (v_D \tau) L^{II} \approx 10^{29}\ \text{electrons} \quad (41)$$

for $(n_{tr}/n)\approx 10^{-3}$, a loop field strength $B \approx 100$ gauss, $L^{II} \approx 10^9$ cm, and a corresponding source lifetime $\tau = L^{II}/c_s \approx 10$ s.

This number is a small fraction of the total number of electrons escaping from region I ($\sim 10^{34}$ s^{-1}) and represents the electron flux responsible for type III emission and the interplanetary stream (Fig. 6). The result is in excellent

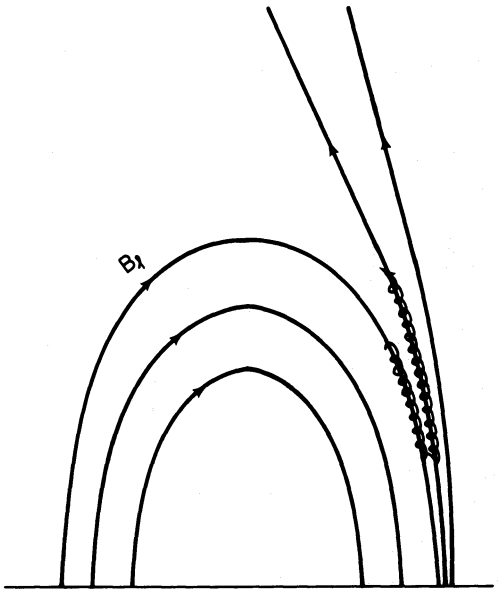

FIG. 6.—Precipitating electrons may drift onto open (or higher closed) field lines as a result of anomalous Doppler resonance interaction between the downward precipitated high energy tail (see Fig. 5) and the background plasma electrons in region II, and be reflected upward along these high field lines. Note that the drift is in the direction $\mathbf{R}\times\mathbf{B}$, where $\mathbf{R}$ is the outward pointing toroidal radius vector, and therefore in fact the electrons drift in a direction *out of the paper* onto the open field lines adjacent to the toroidal closed field lines. These electrons create type III radio bursts and also constitute the stream of electrons observed in interplanetary space (see Lin 1974).

agreement with the work first presented by Kundu (1965) and recently revised by Stewart (1978), who conclude that some 80% of hard X-ray bursts which also have a meter wavelength signature give a special type of type III burst which has a duration $\tau \lesssim 10$ s (compared to the usual 1–2 s in events without hard X-ray signatures). The correlation is not perfect because not all events will have suitable open (or very high closed) field lines to carry the electrons upward into the outer corona.

VIII. SUMMARY AND DISCUSSION

In the preceding sections we have developed in some detail the radiation signatures from a solar flare loop energized locally by a mechanism which was not specified in detail but which was assumed to impulsively heat electrons preferentially over ions. We reiterate here that these two assumptions of *local* and *impulsive electron* heating are both necessary and sufficient for its validity.

A feature of the energy release which was not specified *a priori* but which was deduced from observations (particularly microwave—§ IV) during the impulsive phase of solar flares is the generation of a moderate strength electric field in the energy release region; this electric field accelerates electrons in the energy release region to form a suprathermal tail which precipitates into the denser regions of the loop. The tail can create, through the anomalous Doppler resonance instability, an upward flux of electrons along high, or even open, field lines; such electrons are responsible for type III radio bursts and interplanetary electron streams.

The model has been found to be consistent with observed fluxes and spectra in hard X-rays, microwave, and EUV, and with the observed number of interplanetary electrons. However, only crude estimates of model parameters such as density, temperature, and magnetic field strength have been employed, and it is emphasized that properly coordinated observations, ideally suited to the cooperative Solar Maximum Year program (see Rust and Emslie 1979; Emslie and Rust 1980), are necessary to better define and understand this type of solar flare model. Examples of crucial observations are those of density (see § VI, where upper and lower bounds of 3×10^{10} cm^{-3} and 3×10^{11} cm^{-3} have been imposed herein as constraints based on microwave and hard X-ray observations) and the number of escaping particles (see § VII).

One of the strongest observational predictions of the model is the strong energy dependence of the intrinsic hard X-ray polarization (§ III). Although no polarization measurements capable of testing this prediction yet exist (see Emslie and Brown 1980 and references therein), such measurements are strongly encouraged by the authors, for it

appears that hard X-ray polarization measurements are quite possibly the key to the resolution of the thermal/nonthermal/hybrid (present paper) controversy.

Finally, we again emphasize the strong assumptions we have made concerning the energy release mechanism in the present paper (see § II, assumptions [1] and [2]); the effects of relaxing one or the other of these assumptions merit separate investigation.

We thank J. C. Brown, R. W. Noyes, E. J. Schmahl, D. F. Smith, and P. A. Sturrock for helpful and stimulating discussions on all aspects of the work herein and for comments on the manuscript. During the course of this work, A. G. E. was supported by NAS 5-3949 at the Harvard-Smithsonian Center for Astrophysics, and by ONR N00014-75-C-0673 and NASA NGL 05-020-272 at Stanford University. L. V. was supported by NASA grant NGR 21-002-199 and NSF contract ATM-76-22415-A01.

REFERENCES

Bai, T., and Ramaty, R. 1978, *Ap. J.*, **219**, 705.
Bekefi, G. 1966, *Radiation Processes in Plasmas* (New York: Wiley).
Brown, J. C. 1971, *Solar Phys.*, **18**, 449.
_____. 1972, *Solar Phys.*, **26**, 441.
_____. 1973, *Solar Phys.*, **31**, 143.
_____. 1975, in *IAU Symposium 68, Solar Gamma, X-, and EUV Radiation*, ed. S. R. Kane (Dordrecht: Reidel), p. 245.
Brown, J. C., Canfield, R. C., and Robertson, M. N. 1978, *Solar Phys.*, **57**, 399.
Brown, J. C., Craig, I. J. D., and Karpen, J. T. 1980, *Solar Phys.*, **67**, 143.
Brown, J. C., Melrose, D. B., and Spicer, D. S. 1979, *Ap. J.*, **228**, 592.
Brown, J. C., and Smith, D. F. 1980, *Rept. Prog. Phys.* **43**, 125.
Cheng, C. -C., and Widing, K. G. 1975, *Ap. J.*, **201**, 735.
Crannell, C. J., Frost, K. J., Mätzler, C., Ohki, K., and Saba, J. L. 1978, *Ap. J.*, **223**, 620.
Culhane, J. L., and Acton, L. W. 1970, *M.N.R.A.S.*, **151**, 141.
Donnelly, R. F., and Kane, S. R. 1978, *Ap. J.*, **222**, 1043.
Dulk, G. A., Melrose, D. B., and White, S. M. 1979, *Ap. J.*, **234**, 1137.
Emslie, A. G. 1978, *Ap. J.*, **224**, 241.
_____. 1980, *Ap. J.*, **235**, 1055.
_____. 1981, *Ap. J.*, **243**, in press.
Emslie, A. G., and Brown, J. C. 1980, *Ap. J.*, **237**, 1015.
Emslie, A. G., Brown, J. C., and Donnelly, R. F. 1978, *Solar Phys.*, **57**, 175.
Emslie, A. G., Brown, J. C., and Machado, M. E. 1981, *Ap. J.*, submitted.
Emslie, A. G., and Rust, D. M. 1980, *Solar Phys.*, **65**, 271.
Furth, H. P., Killeen, J., and Rosenbluth, M. N. 1963, *Phys. Fluids*, **6**, 459.
Gradshteyn, I. S., and Rhyzik, I. M. 1965, *Tables of Integrals, Series, and Products* (New York: Interscience).
Guidice, D. A., and Castelli, J. P. 1973, in *High Energy Phenomena on the Sun*, ed. R. Ramaty and R. G. Stone (NASA SP-342), p. 87.
Haber, I., Huba, J. D., Palmadesso, P., and Papadopoulos, K. 1978, *Phys. Fluids*, **21**, 1013.
Heitler, W. 1954, *The Quantum Theory of Radiation* (Oxford: Oxford University Press).
Hénoux, J. -C. 1975, *Solar Phys.*, **42**, 219.
Hoyng, P., Brown, J. C., and van Beek, H. F. 1976, *Solar Phys.*, **48**, 197.
Ionson, J. A. 1976, *Phys. Letters*, **58A**, 105.
Kadomtsev, B. B., and Pogutse, O. P. 1968, *Soviet Phys.—JETP.*, **26**, 1146.
Kahler, S. W. 1971*a*, *Ap. J.*, **164**, 365.
_____. 1971*b*, *Ap. J.*, **168**, 319.
_____. 1975, in *IAU Symposium 68, Solar Gamma, X-, and EUV Radiation*, ed. S. R. Kane (Dordrecht: Reidel), p. 211.
Kane, S. R. 1974, in *IAU Symposium 57, Coronal Disturbances*, ed. G. A. Newkirk, Jr. (Dordrecht: Reidel), p. 105.
Kane, S. R., and Donnelly, R. F. 1971, *Ap. J.*, **164**, 151.
Krall, N. A., and Trivelpiece, A. W. 1973, *Principles of Plasma Physics* (New York: McGraw-Hill).
Kundu, M. R. 1965, *Solar Radio Astronomy* (New York: Interscience).
Langer, S. H., and Petrosian, V. 1977, *Ap. J.*, **215**, 666.
Langer, S. H., Petrosian, V., and Frost, K. J. 1980, *Ap. J.*, **235**, 1047.
Leach, J., and Petrosian, V. 1981, *Ap. J.*, to be submitted.
Lin, R. P. 1974, *Space Sci. Rev.*, **16**, 180.
Lin, R. P., and Hudson, H. S. 1976, *Solar Phys.*, **50**, 153.
Lites, B. W., and Cook, J. W. 1979, *Ap. J.*, **228**, 598.
Liu, C. S., and Mok, Y. C. 1977, *Phys. Rev. Letters*, **38**, 162.
Liu, C. S., Mok, Y. C., Papadopoulos, K., Engleman, F., and Bornatici, M. 1977, *Phys. Rev. Letters*, **39**, 701.
Machado, M. E., Avrett, E. H., Vernazza, J. E., and Noyes, R. W. 1980, *Ap. J.*, **242**, in press.
Machado, M. E., and Emslie, A. G. 1979, *Ap. J.*, **232**, 903.
Machado, M. E., and Linsky, J. L. 1975, *Solar Phys.*, **42**, 295.
Manheimer, W. M. 1977, *Phys. Fluids*, **20**, 265.
Mätzler, C. 1978, *Astr. Ap.*, **70**, 181.
Mätzler, C., Bai, T., Crannell, C. J., and Frost, K. J. 1978, *Ap. J.*, **223**, 1058.
Petrosian, V. 1973, *Ap. J.*, **186**, 291.
Ramaty, R. 1969, *Ap. J.*, **158**, 753.
_____. 1973, in *High Energy Phenomena on the Sun*, ed. R. Ramaty and R. G. Stone (NASA SP-342), p. 188.
Rudakov, L. I., and Korablev, A. B. 1966, *Zh. Eksper. Theor. Fis.*, **50**, 220.
Rust, D. M., and Emslie, A. G. (eds.). 1979, *Energy Release in Solar Flares* (Boulder: WDCA Report UAG-72).
Smith, D. F., and Auer, L. H. 1980, *Ap. J.*, **238**, 1126.
Smith, D. F., and Brown, J. C. 1980, *Ap. J.*, **242**, in press.
Smith, D. F., and Lilliequist, C. G. 1979, *Ap. J.*, **232**, 582.
Somov, B. V. 1975, *Solar Phys.*, **42**, 225.
_____. 1979, *Solar Phys.*, **60**, 315.
Spicer, D. S. 1976, N.R.L. Report 8036.
_____. 1977*a*, *Solar Phys.*, **53**, 305.
_____. 1977*b*, *Solar Phys.*, **54**, 379.
Spitzer, L. W. 1962, *Physics of Fully Ionized Gases* (New York: Interscience).
Stewart, R. T. 1978, *Solar Phys.*, **58**, 121.
Sturrock, P. A. (ed.). 1980, *Solar Flares—A Monograph from Skylab Solar Workshop II* (Boulder: University of Colorado Press).
Švestka, Z. 1976, *Solar Flares* (Dordrecht: Reidel).
Takakura, T. 1972, *Solar Phys.*, **26**, 151.
Van Hoven, G. 1979, *Ap. J.*, **232**, 572.
Vlahos, L. 1979, Ph.D. thesis, University of Maryland.
Vlahos, L., and Papadopoulos, K. 1979, *Ap. J.*, **233**, 717 (VP).
Widing, K. G., and Cheng, C. -C. 1974, *Ap. J.* (*Letters*), **144**, L111.

A. Gordon Emslie: Institute for Plasma Research, Stanford University, Via Crespi, Stanford, CA 94305

Loukas Vlahos: Astronomy Program, Space Sciences Bld., University of Maryland, College Park, MD 20742